Supplemental information

Tuning the structure of bifunctional Pt/$SmMn_2O_5$ interface for promoted low-temperature CO oxidation activity

Xiao Liu,[a] Jiaqiang Yang,[b] Gurong Shen,[c] Meiqing Shen,[c] Yunkun Zhao,[d] Kyeongjae Cho,[e] Bin Shan,[*b,e] and Rong Chen[*a]

[a]*State Key Laboratory of Digital Manufacturing Equipment and Technology and School of Mechanical Science and Engineering, Huazhong University of Science and Technology, Wuhan 430074, Hubei, People's Republic of China*

[b]*State Key Laboratory of Materials Processing and Die and Mould Technology and School of Materials Science and Engineering, Huazhong University of Science and Technology, Wuhan 430074, Hubei, People's Republic of China*

[c]*School of Materials Science and Engineering, Tianjin University, Tianjin 300072, People's Republic of China*

[d]*State Key Laboratory of Advanced Technologies for Comprehensive Utilization of Platinum Metal, Kunming Institute of Precious Metals, Kunming 650106, Yunnan, People's Republic of China*

[e]*Department of Materials Science and Engineering, The University of Texas at Dallas, Richardson, Texas 75080, United States*

Corresponding authors: rongchen@mail.hust.edu.cn (Rong Chen) and bshan@mail.hust.edu.cn (Bin Shan)

Supplementary details of microkinetic analysis

The full catalytic cycle includes the following equations:

$$2\mathrm{CO}(g) + *_{\mathrm{Pt/Mn\text{-}X}} \underset{k_{-1}}{\overset{k_{\mathrm{ads1}}}{\rightleftharpoons}} \mathrm{CO_{Pt}}\sim\mathrm{CO_{Pt}}\sim* \qquad \text{(step i to ii)}$$

$$\mathrm{O_2}(g) + \mathrm{CO_{Pt}}\sim\mathrm{CO_{Pt}}\sim* \underset{k_{-2}}{\overset{k_{\mathrm{ads2}}}{\rightleftharpoons}} \mathrm{CO_{Pt}}\sim\mathrm{CO_{Pt}}\sim\mathrm{O_2}^* \qquad \text{(step ii to iii)}$$

$$\mathrm{CO_{Pt}}\sim\mathrm{CO_{Pt}}\sim\mathrm{O_2}^* \underset{k_{-3}}{\overset{k_3}{\rightleftharpoons}} \mathrm{CO_{Pt}}\sim\mathrm{CO_{Pt}}\sim\mathrm{O}^*\sim\mathrm{O}^* \qquad \text{(step iii to iv)}$$

$$\mathrm{CO_{Pt}}\sim\mathrm{CO_{Pt}}\sim\mathrm{O}^*\sim\mathrm{O}^* \underset{k_{-4}}{\overset{k_4}{\rightleftharpoons}} \mathrm{CO_{Pt}}\sim\mathrm{O}^*\sim\mathrm{CO_2}^* \qquad \text{(step iv to v)}$$

$$\mathrm{CO_{Pt}}\sim\mathrm{O}^*\sim\mathrm{CO_2}^* \underset{k_{-5}}{\overset{k_5}{\rightleftharpoons}} \mathrm{CO_{Pt}}\sim\mathrm{O}^* + \mathrm{CO_2}(g) \qquad \text{(step v to vi)}$$

$$\mathrm{CO_{Pt}}\sim\mathrm{O}^* \underset{k_{-6}}{\overset{k_6}{\rightleftharpoons}} \mathrm{CO_2}^* \qquad \text{(step vi to vii)}$$

$$\mathrm{CO_2}^* \underset{k_{-7}}{\overset{k_7}{\rightleftharpoons}} *_{\mathrm{Pt/Mn\text{-}X}} + \mathrm{CO_2}(g) \qquad \text{(step vii to i)}$$

The corresponding reaction rates (r_i) for each step in the full catalytic cycle are calculated as:

$$r_1 = k_{\mathrm{ads1}} * p(\mathrm{CO})^2 * \theta_{*_{\mathrm{Pt/Mn\text{-}X}}} - k_{-1} * \theta_{\mathrm{CO_{Pt}}\sim\mathrm{CO_{Pt}}\sim*} = k_{\mathrm{ads1}} * p(\mathrm{CO})^2 * \theta_{*_{\mathrm{Pt/Mn\text{-}X}}}(1 - x_1) \qquad (1)$$

$$r_2 = k_{\mathrm{ads2}} * p(\mathrm{O_2}) * \theta_{\mathrm{CO_{Pt}}\sim\mathrm{CO_{Pt}}\sim*} - k_{-2} * \theta_{\mathrm{CO_{Pt}}\sim\mathrm{CO_{Pt}}\sim\mathrm{O_2}*} = k_{\mathrm{ads2}} * p(\mathrm{O_2}) * \theta_{\mathrm{CO_{Pt}}\sim\mathrm{CO_{Pt}}\sim*}(1 - x_2) \qquad (2)$$

$$r_3 = k_3 * \theta_{\mathrm{CO_{Pt}}\sim\mathrm{CO_{Pt}}\sim\mathrm{O_2}*} - k_{-3} * \theta_{\mathrm{CO_{Pt}}\sim\mathrm{CO_{Pt}}\sim\mathrm{O}*\sim\mathrm{O}*} = k_3 * \theta_{\mathrm{CO_{Pt}}\sim\mathrm{CO_{Pt}}\sim\mathrm{O_2}*}(1 - x_3) \qquad (3)$$

$$r_4 = k_4 * \theta_{\mathrm{CO_{Pt}}\sim\mathrm{CO_{Pt}}\sim\mathrm{O}*\sim\mathrm{O}*} - k_{-4} * \theta_{\mathrm{CO_{Pt}}\sim\mathrm{O}*\sim\mathrm{CO_2}*} = k_4 * \theta_{\mathrm{CO_{Pt}}\sim\mathrm{CO_{Pt}}\sim\mathrm{O}*\sim\mathrm{O}*}(1 - x_4) \qquad (4)$$

$$r_5 = k_5 * \theta_{\mathrm{CO_{Pt}}\sim\mathrm{O}*\sim\mathrm{CO_2}*} - k_{-5} * \theta_{\mathrm{CO_{Pt}}\sim\mathrm{O}*} * p(\mathrm{CO_2}) = k_5 * \theta_{\mathrm{CO_{Pt}}\sim\mathrm{O}*\sim\mathrm{CO_2}*}(1 - x_5) \qquad (5)$$

$$r_6 = k_6 * \theta_{\mathrm{CO_{Pt}}\sim\mathrm{O}*} - k_{-6} * \theta_{\mathrm{CO_2}*} = k_6 * \theta_{\mathrm{CO_{Pt}}\sim\mathrm{O}*}(1 - x_6) \qquad (6)$$

$$r_7 = k_7 * \theta_{\mathrm{CO_2}*} - k_{-7} * \theta_{*_{\mathrm{Pt/Mn\text{-}X}}} * p(\mathrm{CO_2}) = k_7 * \theta_{\mathrm{CO_2}*}(1 - x_7) \qquad (7)$$

where x_1~x_7 are defined as:

$$x_1 = \frac{k_{-1} * \theta_{\mathrm{CO_{Pt}}\sim\mathrm{CO_{Pt}}\sim*}}{k_{\mathrm{ads1}} * p(\mathrm{CO})^2 * \theta_{*_{\mathrm{Pt/Mn\text{-}X}}}} \qquad (8)$$

$$x_2 = \frac{k_{-2} * \theta_{\mathrm{CO_{Pt}}\sim\mathrm{CO_{Pt}}\sim\mathrm{O_2}*}}{k_{\mathrm{ads2}} * p(\mathrm{O_2}) * \theta_{\mathrm{CO_{Pt}}\sim\mathrm{CO_{Pt}}\sim*}} \qquad (9)$$

$$x_3 = \frac{k_{-3} * \theta_{\mathrm{CO_{Pt}}\sim\mathrm{CO_{Pt}}\sim\mathrm{O}*\sim\mathrm{O}*}}{k_3 * \theta_{\mathrm{CO_{Pt}}\sim\mathrm{CO_{Pt}}\sim\mathrm{O_2}*}} \qquad (10)$$

$$x_4 = \frac{k_{-4} * \theta_{CO_{Pt}\sim O^*\sim CO_2^*}}{k_4 * \theta_{CO_{Pt}\sim CO_{Pt}\sim O^*\sim O^*}} \tag{11}$$

$$x_5 = \frac{k_{-5} * \theta_{CO_{Pt}\sim O^*} * p(CO_2)}{k_5 * \theta_{CO_{Pt}\sim O^*\sim CO_2^*}} \tag{12}$$

$$x_6 = \frac{k_{-6} * \theta_{CO_2^*}}{k_6 * \theta_{CO_{Pt}\sim O^*}} \tag{13}$$

$$x_7 = \frac{k_{-7} * \theta_{*_{Pt/Mn\text{-}X}} * p(CO_2)}{k_7 * \theta_{CO_2^*}} \tag{14}$$

r_i are solved based on the mean-field steady-state condition ($\frac{\partial \theta}{\partial t} = 0$). The set of master equations is listed as (15)~(22).

$$\frac{\partial \theta_{*_{Pt/Mn\text{-}X}}}{\partial t} = 0 \Rightarrow r_7 - r_1 = 0 \tag{15}$$

$$\frac{\partial \theta_{CO_{Pt}\sim CO_{Pt}\sim^*}}{\partial t} = 0 \Rightarrow r_1 - r_2 = 0 \tag{16}$$

$$\frac{\partial \theta_{CO_{Pt}\sim CO_{Pt}\sim O_2^*}}{\partial t} = 0 \Rightarrow r_2 - r_3 = 0 \tag{17}$$

$$\frac{\partial \theta_{CO_{Pt}\sim CO_{Pt}\sim O^*\sim O^*}}{\partial t} = 0 \Rightarrow r_3 - r_4 = 0 \tag{18}$$

$$\frac{\partial \theta_{CO_{Pt}\sim O^*\sim CO_2^*}}{\partial t} = 0 \Rightarrow r_4 - r_5 = 0 \tag{19}$$

$$\frac{\partial \theta_{CO_{Pt}\sim O^*}}{\partial t} = 0 \Rightarrow r_5 - r_6 = 0 \tag{20}$$

$$\frac{\partial \theta_{CO_2^*}}{\partial t} = 0 \Rightarrow r_6 - r_7 = 0 \tag{21}$$

$$x_7 x_1 x_2 x_3 x_4 x_5 x_6 = \frac{k_{-1} k_{-2} k_{-3} k_{-4} k_{-5} k_{-6} k_{-7} * p(CO_2)^2}{k_{ads1} k_{ads2} k_3 k_4 k_5 k_6 k_7 * p(CO)^2 * p(O_2)} \tag{22}$$

Since the sequential steps after O_2 dissociation are strongly exothermic with much low barrier energies, we have assumed the adsorption of CO and O_2 in equilibrium and the rate of CO_2 formation (r) is equal to the rate of O_2 dissociation.

Therefore, the equilibrium constants (K_1 and K_2) can be written as:

$$K_1 = \frac{k_{\text{ads1}}}{k_{-1}} = \frac{\theta_{\text{CO}_{\text{Pt}}\sim\text{CO}_{\text{Pt}}\sim *}}{p(\text{CO})^2 * \theta_{*_{\text{Pt/Mn-X}}}} \tag{23}$$

$$K_2 = \frac{k_{\text{ads2}}}{k_{-2}} = \frac{\theta_{\text{CO}_{\text{Pt}}\sim\text{CO}_{\text{Pt}}\sim\text{O}_2 *}}{p(\text{O}_2) * \theta_{\text{CO}_{\text{Pt}}\sim\text{CO}_{\text{Pt}}\sim *}} \tag{24}$$

The site balance at the interface leads to the following equation of the coverages of species.

$$\theta_{*_{\text{Pt/Mn-X}}} + \theta_{\text{CO}_{\text{Pt}}\sim\text{CO}_{\text{Pt}}\sim *} + \theta_{\text{CO}_{\text{Pt}}\sim\text{CO}_{\text{Pt}}\sim\text{O}_2 *} = 1 \tag{25}$$

Therefore, *r* can be calculated as:

$$r = k_3 * \theta_{\text{CO}_{\text{Pt}}\sim\text{CO}_{\text{Pt}}\sim\text{O}_2^*} = \frac{k_3 K_1 K_2 p(\text{CO})^2 p(\text{O}_2)}{1 + K_1 p(\text{CO})^2 + K_1 K_2 p(\text{CO})^2 p(\text{O}_2)} \tag{26}$$

Fig. S1

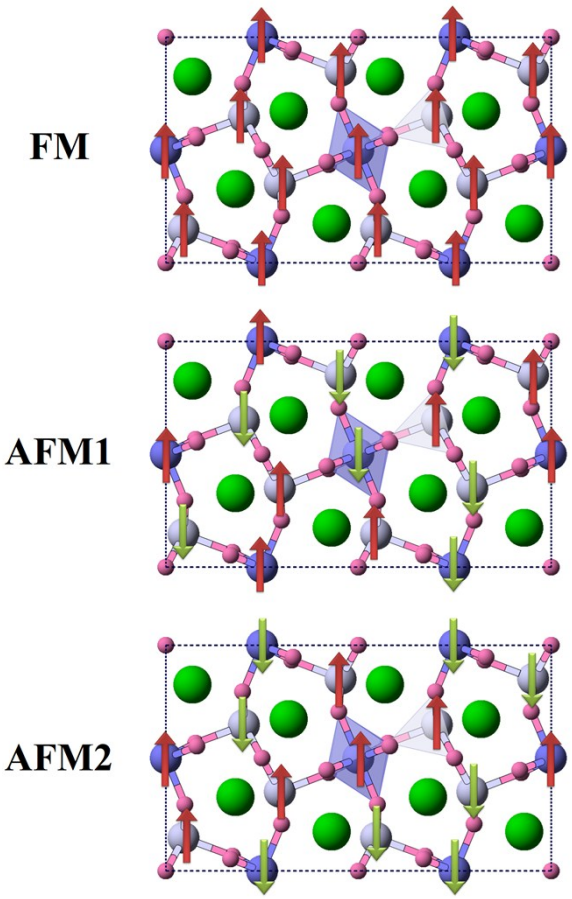

Fig. S1 The detailed configurations of initial magnetic moment for each Mn atom under ferromagnetic (FM) and antiferromagnetic (AFM) states. The listed results in Table S1 showed that the AFM1 state is the ground state with the total energy of -531.09 eV and the optimized lattice constants of 2a = 1.464 nm, b = 0.859 nm, c = 0.568 nm.

Fig. S2

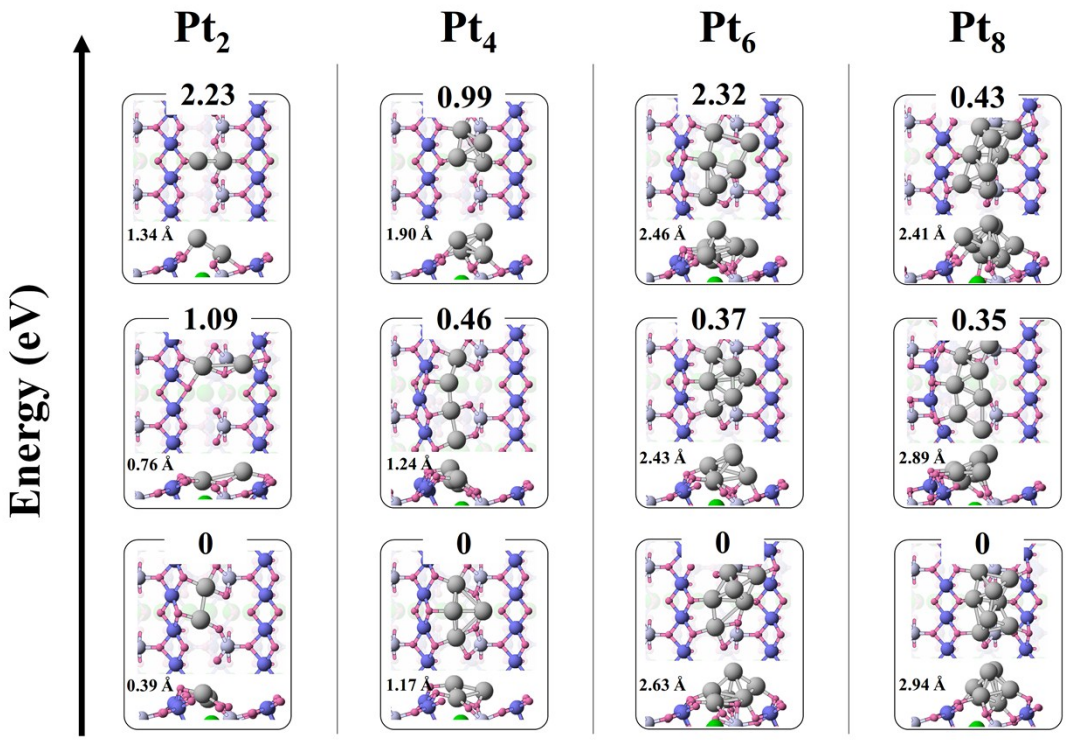

Fig. S2 The optimized structures of Pt_n/SMO (n = 2, 4, 6 and 8). The clustering energies have been labeled, which are relative to the most stable configurations. The heights between bottom and top Pt atoms ($h_{Pt\text{-}Pt}$) have been labeled, which shows that the smaller $h_{Pt\text{-}Pt}$s can lead to more stable configurations for Pt_2 and Pt_4. On the contrary, the larger $h_{Pt\text{-}Pt}$s for Pt_6 and Pt_8 can result to more stable configurations.

Fig. S3

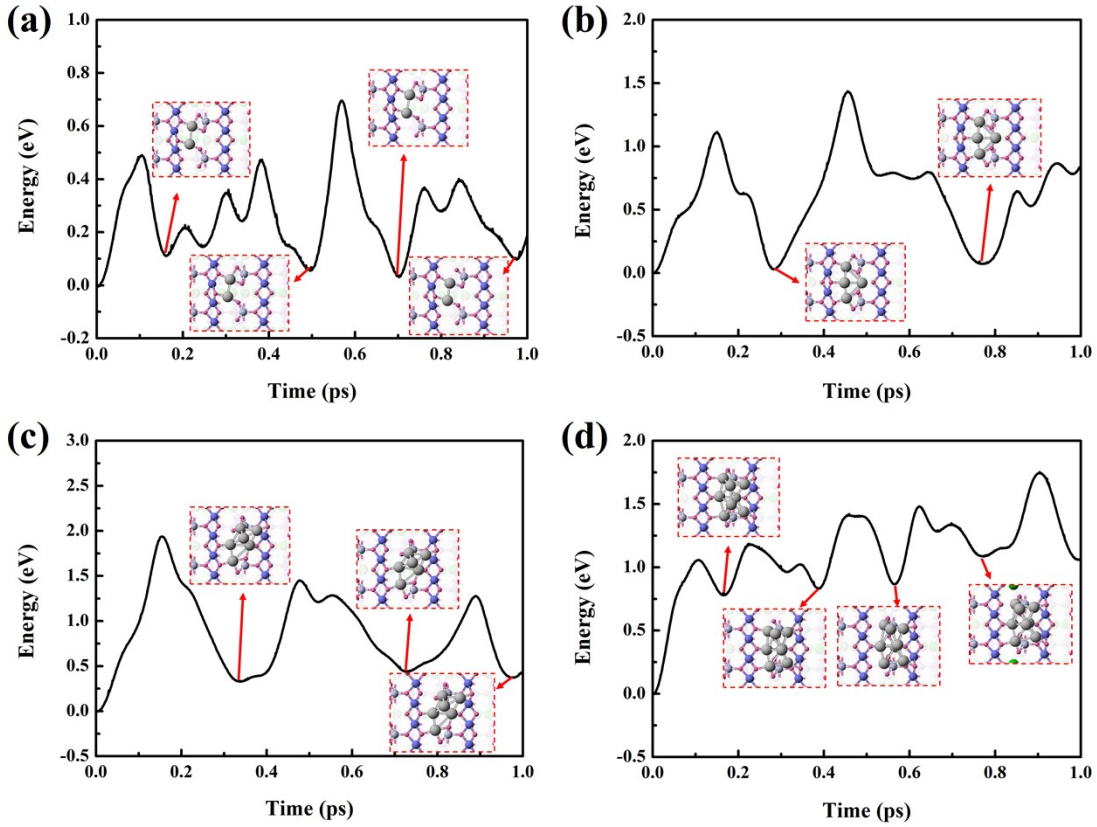

Fig. S3 The total energies of Pt_n/SMO (n = 2, 4, 6 and 8) as a function of simulation time during the first-principle molecular dynamic simulations at 973 K. The inserted figures are the snapshots of Pt_n/SMO with the local minimum total energies.

Fig. S4

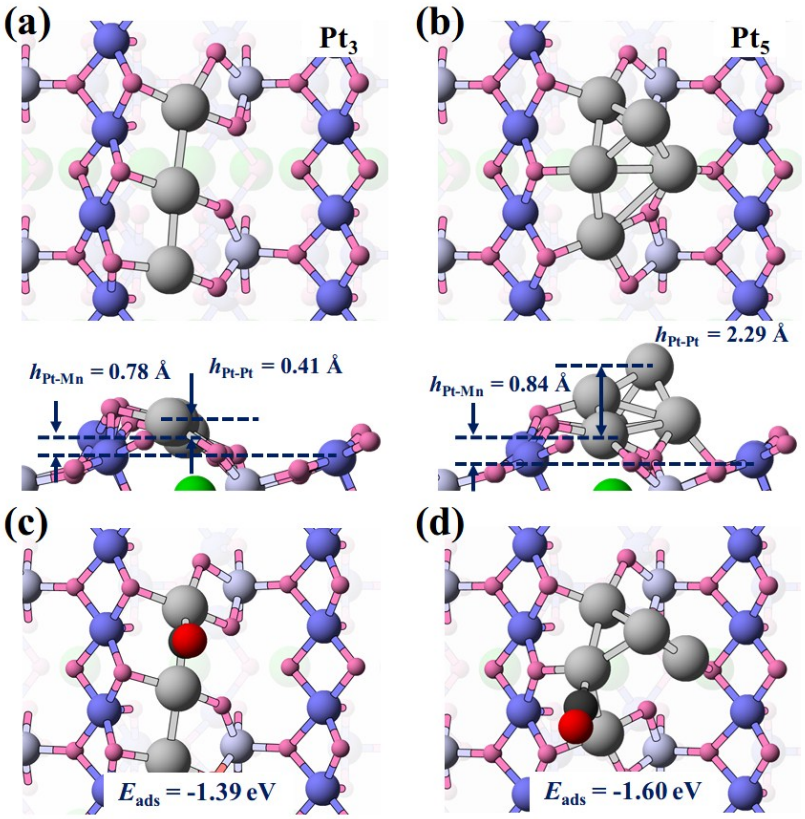

Fig. S4 Top view and side view of the most stable configurations of (a) Pt_3 and (b) Pt_5 clusters on SMO surface. Atomic structures of SMO supported (c) Pt_3 and (d) Pt_5 clusters with an adsorbed CO molecule.

Fig. S5

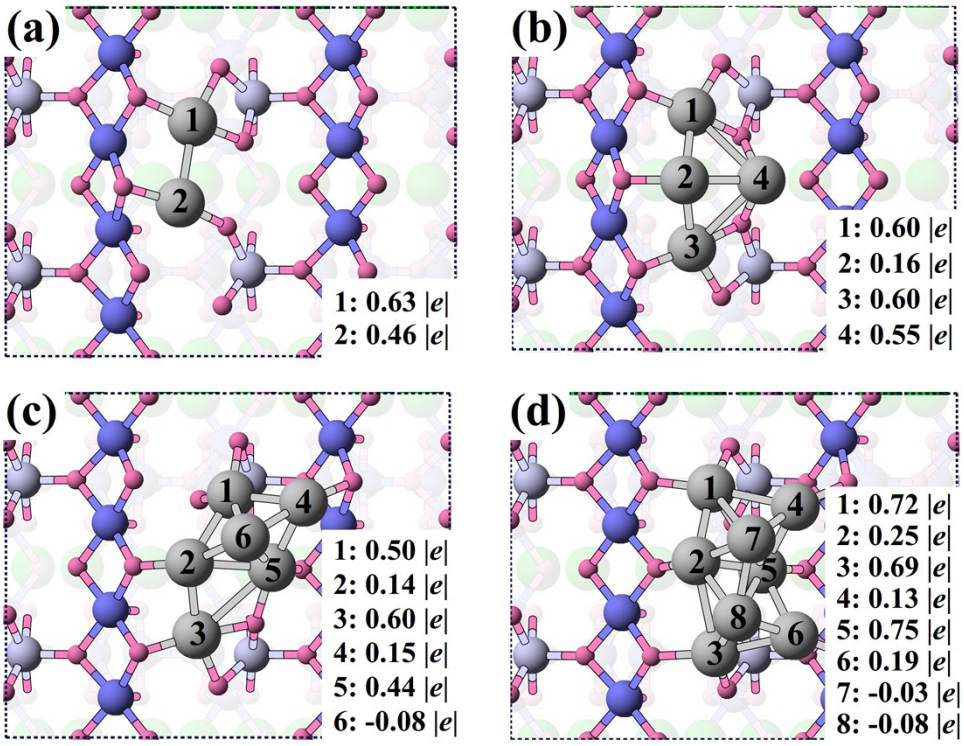

Fig. S5 The Bader charges of Pt atoms for Pt_n/SMO (n = 2, 4, 6 and 8) with the most stable structure.

Fig. S6

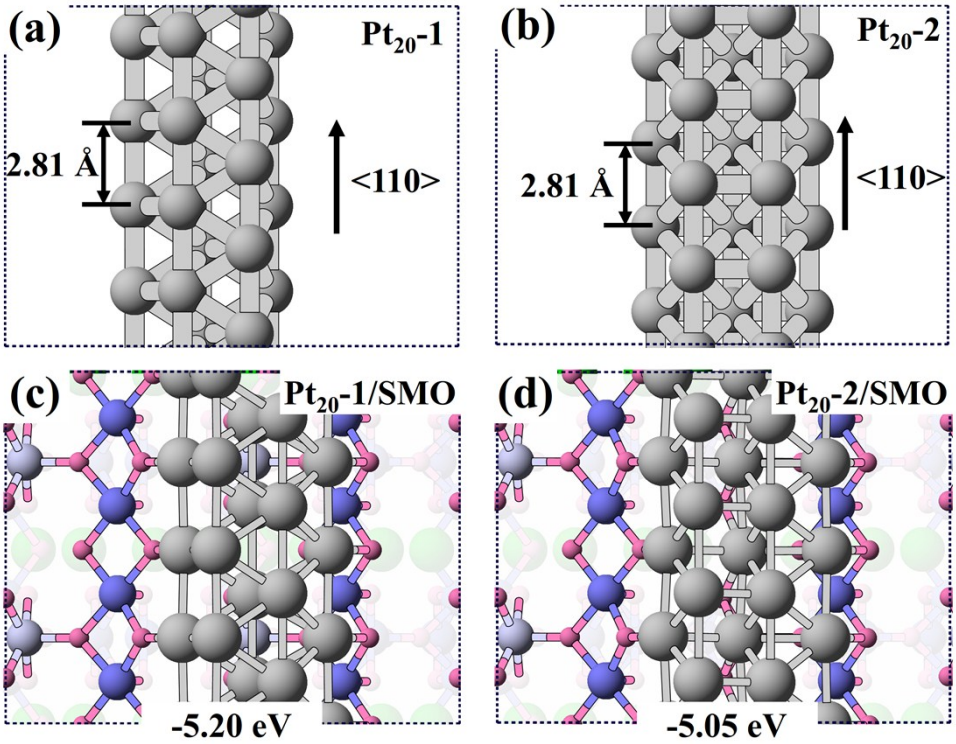

Fig. S6 (a)(b) The atomic structures of two types of rod-like Pt_{20} clusters along <110> direction. The optimized atomic structures of (c) Pt_{20}-1 and (d) Pt_{20}-2 bound on SMO (010) facet are presented with the clustering energies labeled at the bottom.

Fig. S7

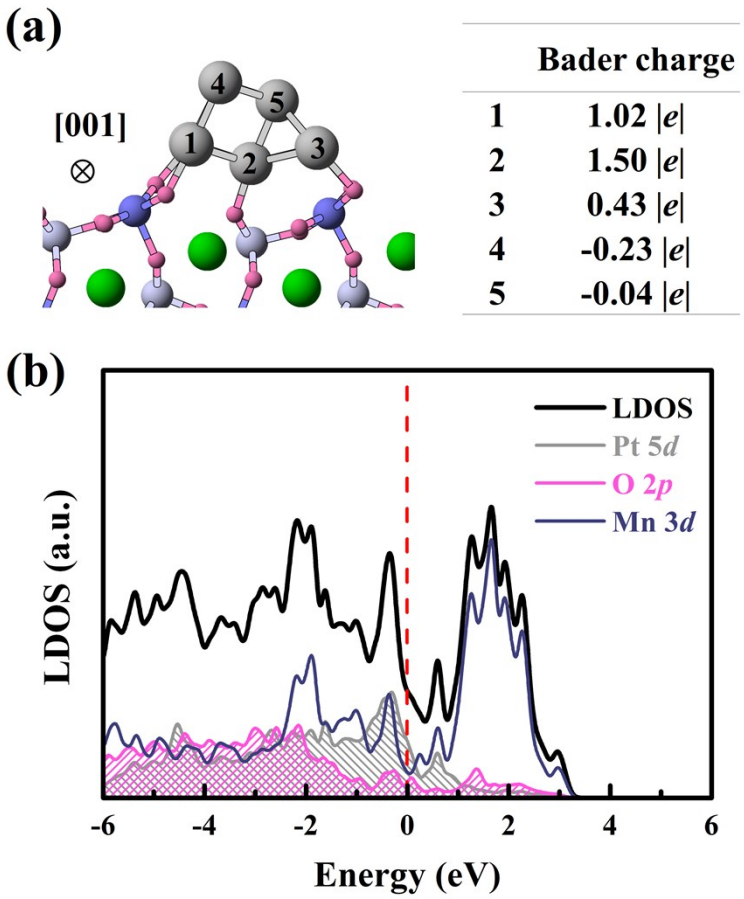

Fig. S7 (a) The Bader charges for the overlapped Pt atoms in [001] direction of Pt_{20}/SMO. (b) The LDOS and partial DOS for Pt 5*d*, O 2*p* and Mn 3*d* of the Pt/Mn_2 trimer interface of Pt_{20}/SMO.

Fig. S8

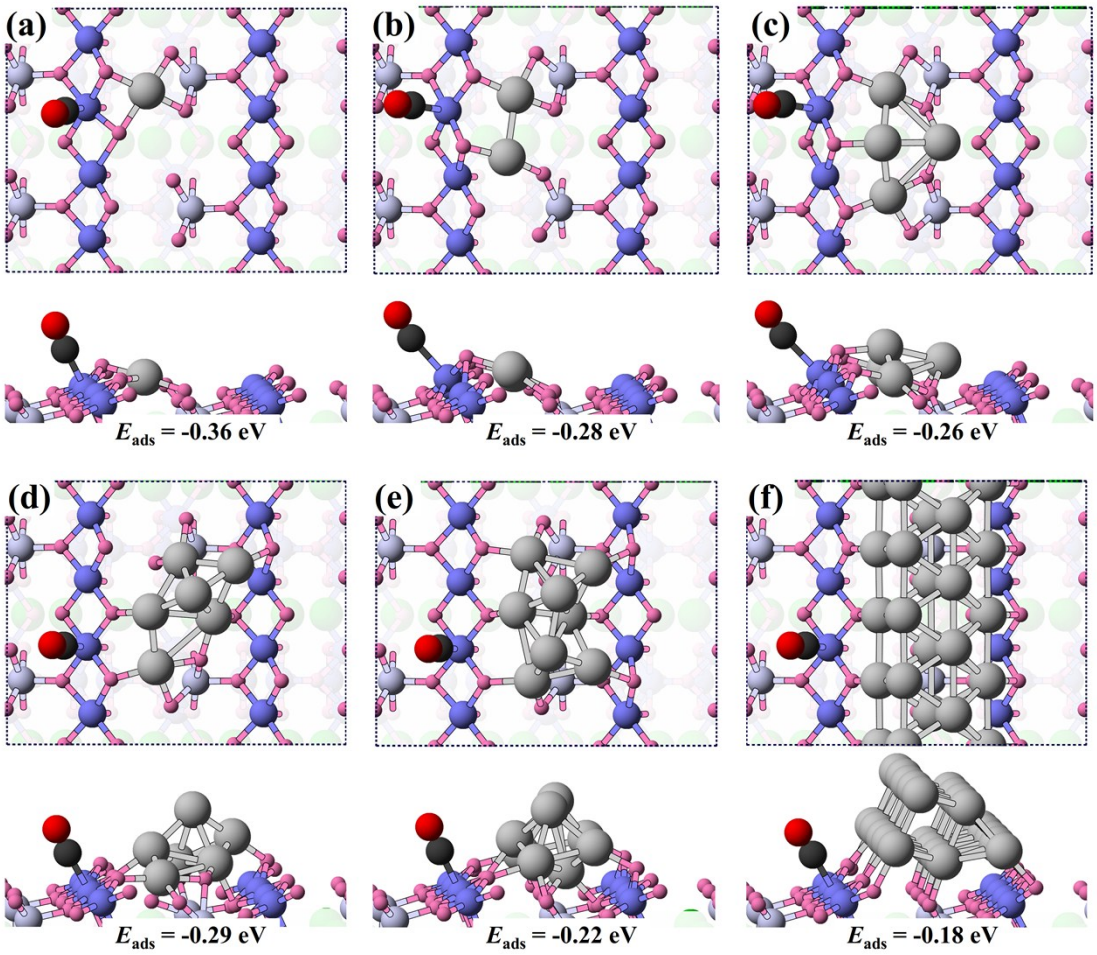

Fig. S8 The atomic structures of CO adsorption on Mn_2 dimer site of Pt_n/SMO (n = 1, 2, 4, 6, 8 and 20). The calculated adsorption energy ranges from -0.18 eV to -0.36 eV, which indicates the weakly physical adsorption of CO on the Mn_2 dimer site.

Fig. S9

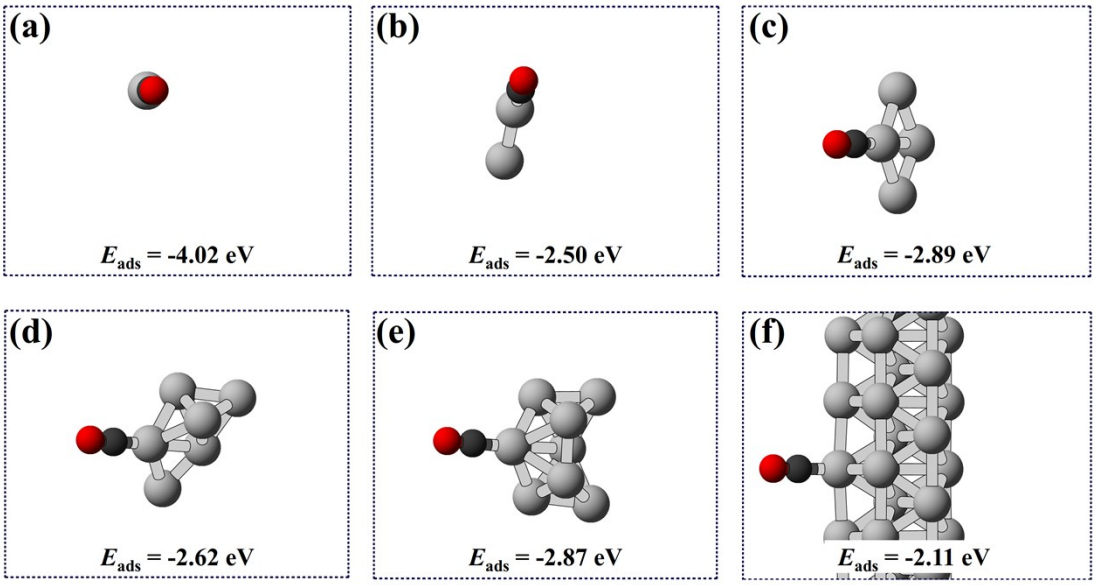

Fig. S9 The atomic structures of CO adsorption on isolated Pt clusters with the corresponding adsorption energies labeled at the bottom.

Fig. S10

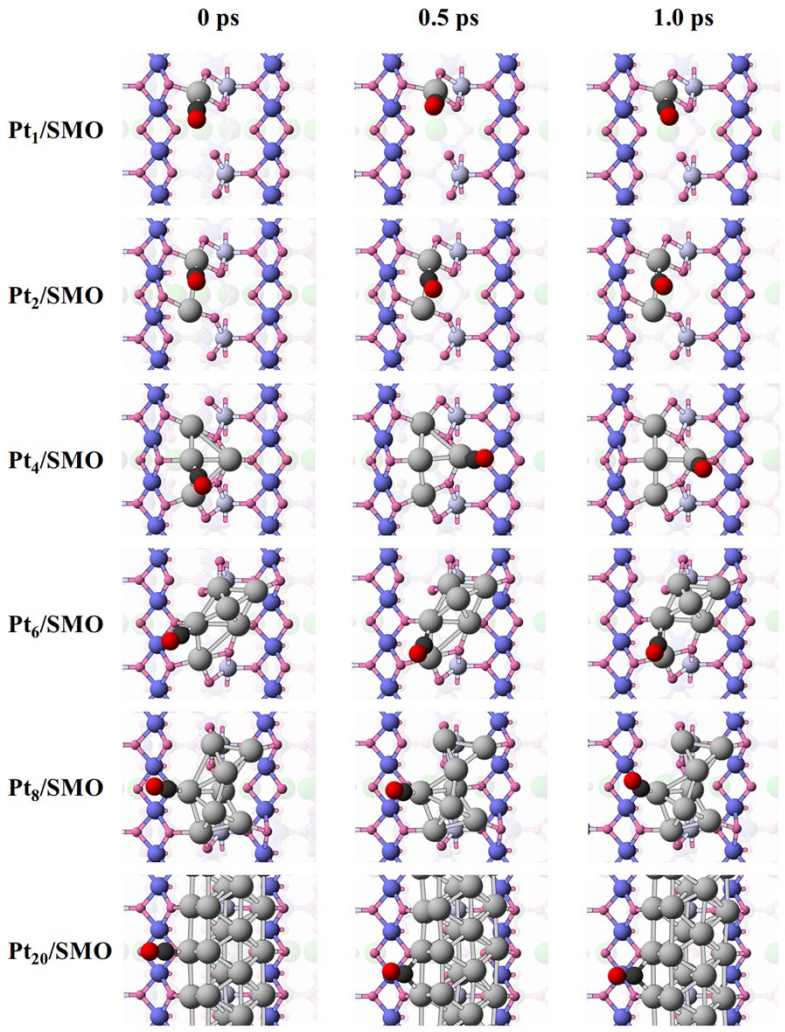

Fig. S10 Simulation snapshots for the evolution of CO adsorbed Pt_n/SMO (n = 1, 2, 4, 6, 8 and 20) at 473 K.

Fig. S11

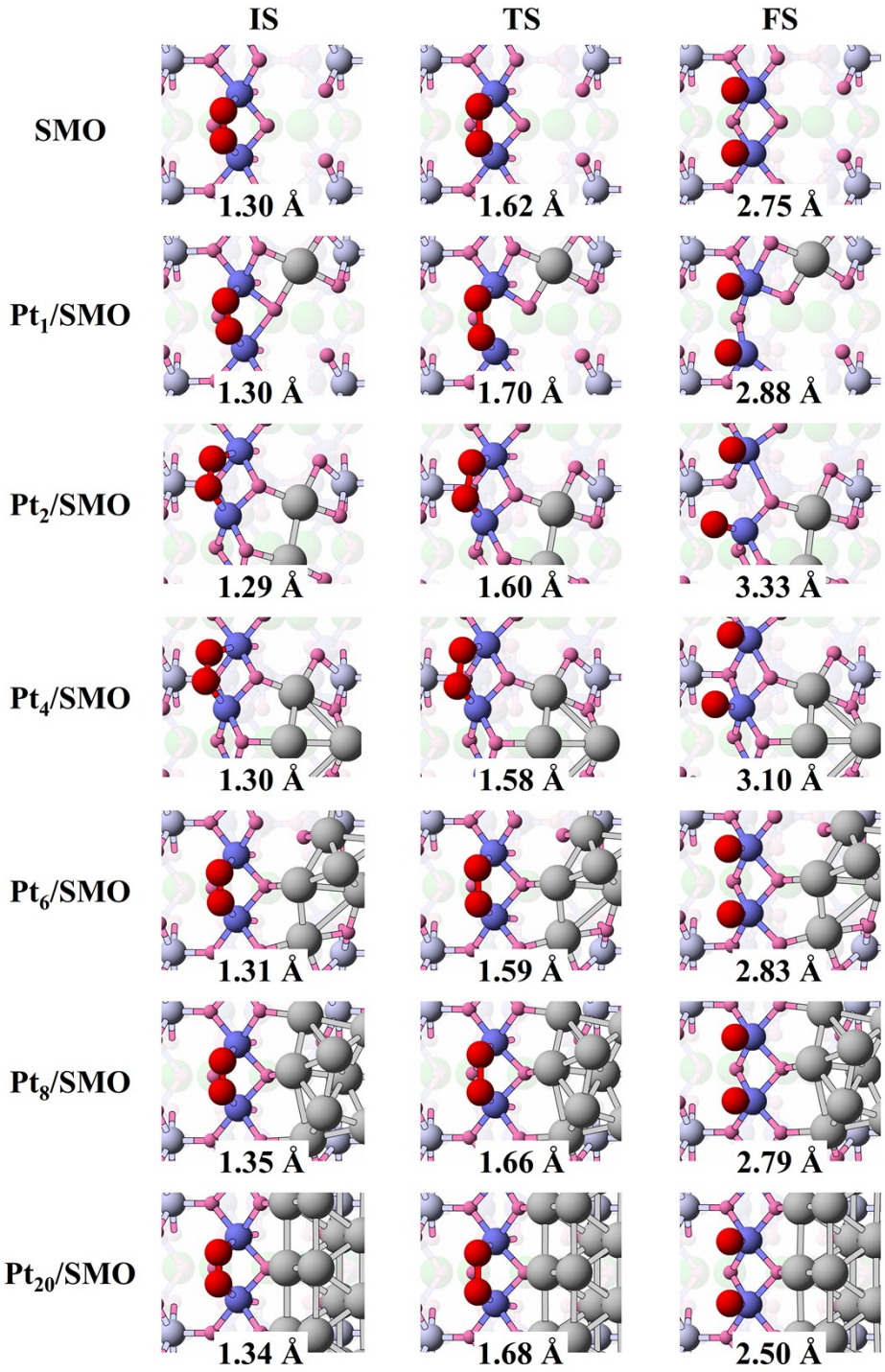

Fig. S11 The atomic structures of the initial states (IS), the transition states (TS) and the final states (FS) of O_2 dissociation on the Mn_2 dimer sites of bare SMO (010) facet and Pt_n/SMO. The distances between O atoms are labeled.

Fig. S12

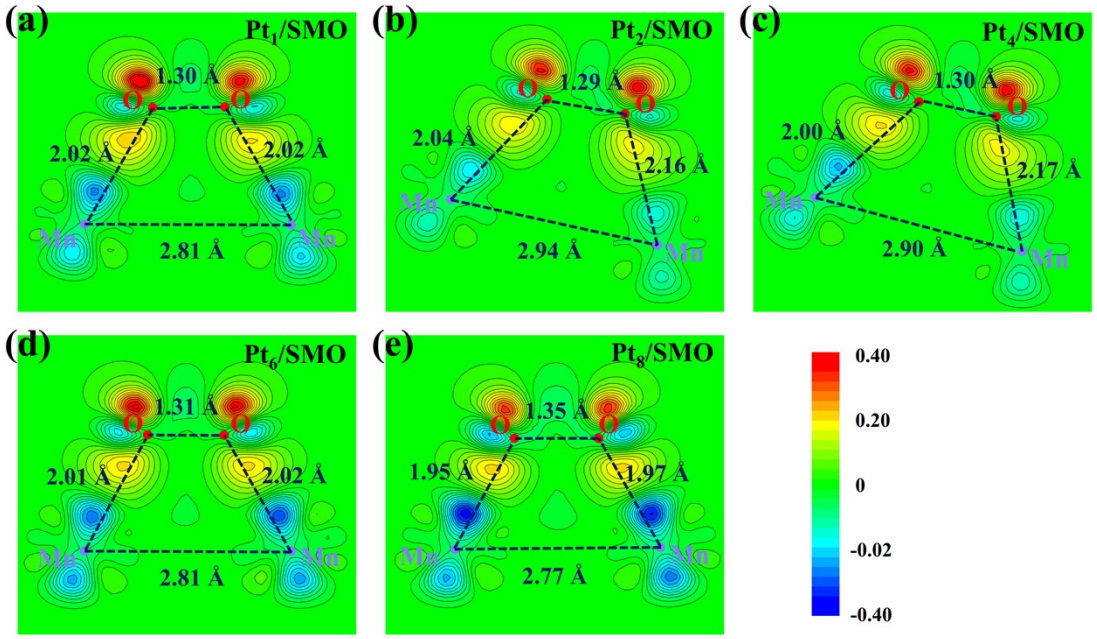

Fig. S12 The contours of the differential charge density in the plane crossing the adsorbed O_2 molecule and Mn_2 dimer for (a) Pt_1/SMO, (b) Pt_2/SMO, (c) Pt_4/SMO, (d) Pt_6/SMO and (e) Pt_8/SMO. The distances (Å) between two neighbor atoms have been labeled.

Fig. S13

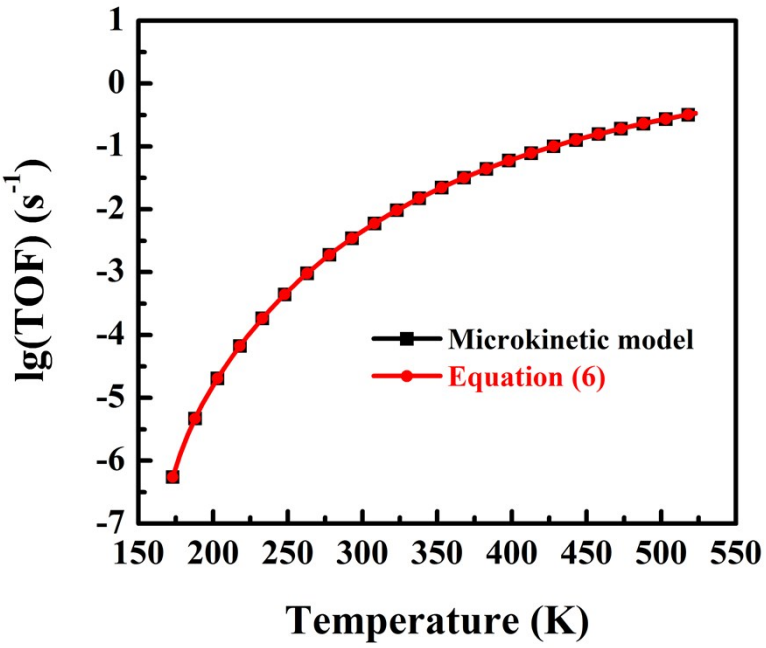

Fig. S13 TOF calculated by the set of master equations of microkinetic model (black curve) and equation (6) in the text (red curve) as a function of reaction temperature.

Fig. S14

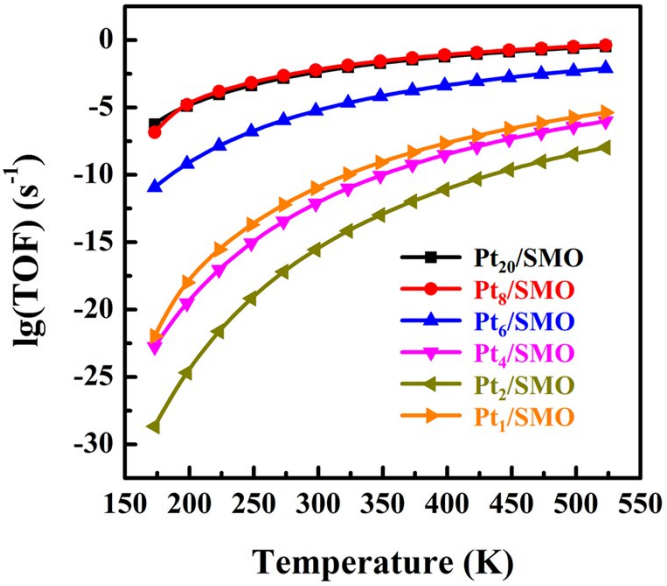

Fig. S14 TOF as a functional of reaction temperature for Pt_n/SMO (n = 1, 2, 4, 6, 8 and 20).

Fig. S15

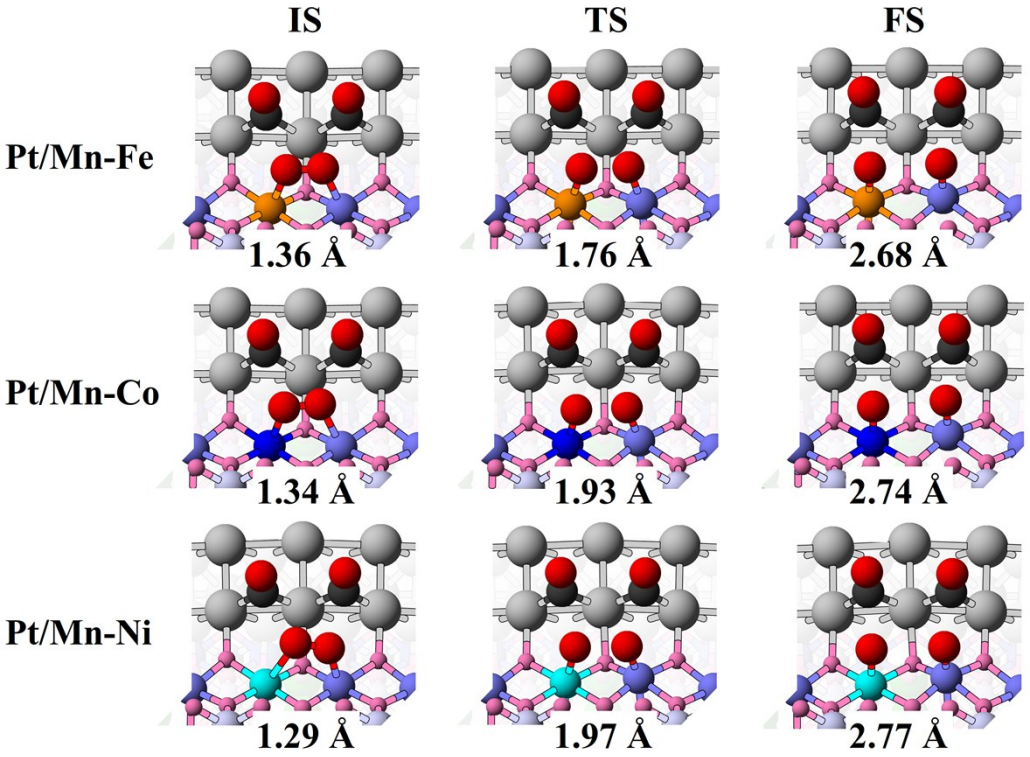

Fig. S15 The atomic structures of the initial states (IS), the transition states (TS) and the final states (FS) of O_2 dissociation on the Mn-Fe, Mn-Co and Mn-Ni hetero-dimer sites of Pt_{20}/SMO. Note that the pre-adsorbed CO molecules on the interfacial Pt sites have been considered due to their effects on the adsorption energy of O_2 on Mn dimer as discussed in the text. The distances between O atoms are labeled.

Fig. S16

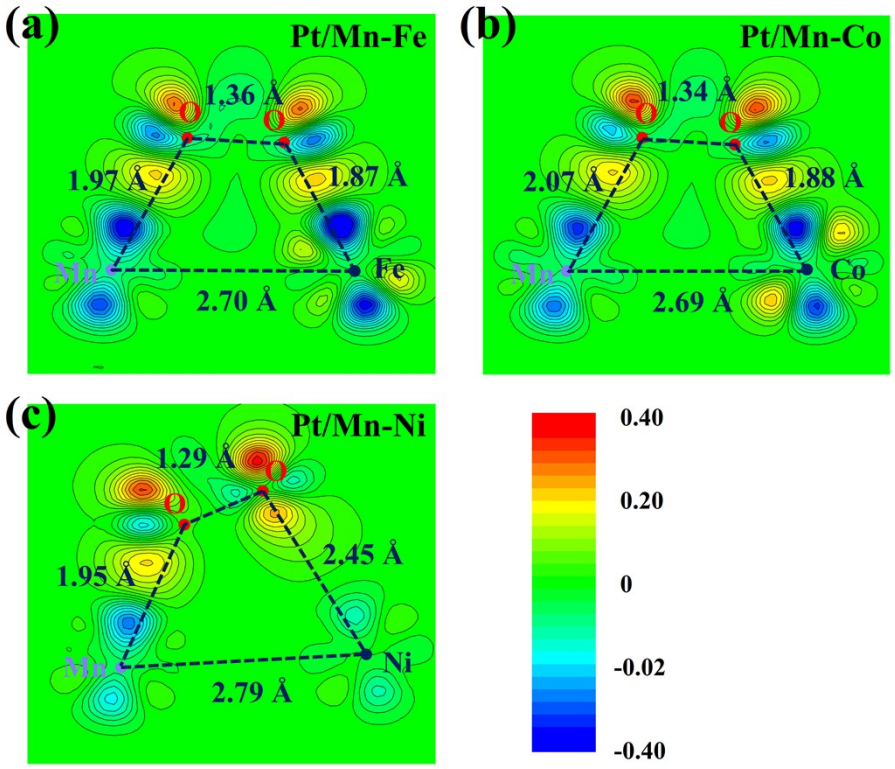

Fig. S16 The contours of the differential charge density in the plane crossing the adsorbed O_2 molecule and (a) Mn-Fe, (b) Mn-Co, (c) Mn-Ni hetero-dimers for Pt_{20}/SMO. The distances (Å) between two neighbor atoms have been labeled.

Fig. S17

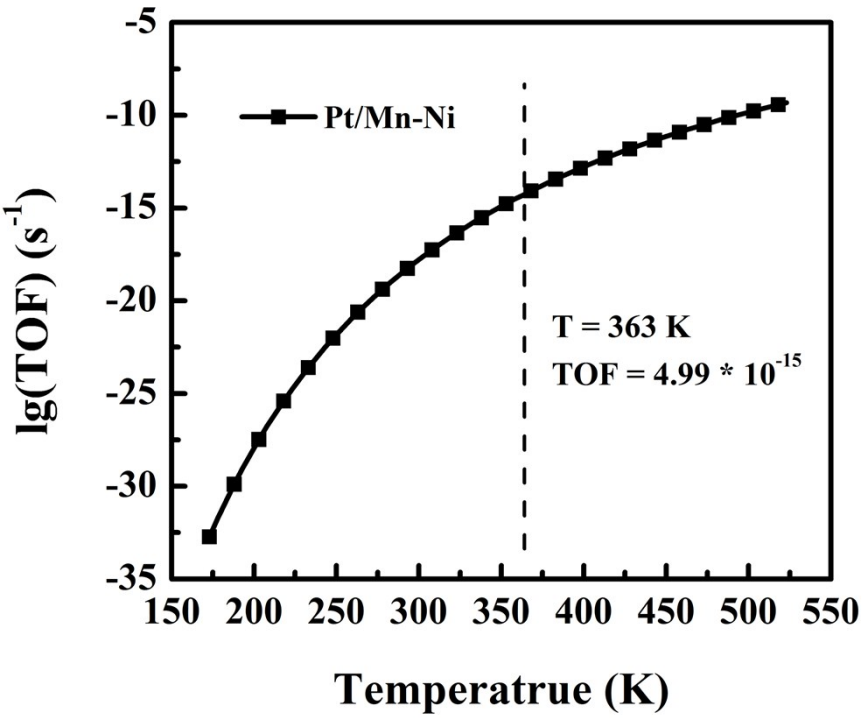

Fig. S17 TOF as a function of reaction temperature for Pt/Mn-Ni trimer interface. The calculated TOF at 363 K are labelled.

Table S1 The optimized lattice constants, total energies and total magnetic moment of SMO bulk calculated with different initial magnetic states. The corresponding data in previous experimental study have also been listed for comparison.

	FM	AFM1	AFM2	exp.[a]
2a (Å)	14.666	14.645	14.640	14.85
b (Å)	8.574	8.590	8.578	8.596
c (Å)	5.722	5.676	5.697	5.672
E (eV)	-530.09	-531.09	-530.76	/
mag (μ_B)	55.95	0	0	0

[a] Y. Ishii, S. Horio, M. Mitarashi, T. Sakakura, M. Fukunaga, Y. Noda, T. Honda, H. Nakao, Y. Murakami and H. Kimura, *Phys. Rev. B*, 2016, **93**, 064415.

Table S2. Adsorption energies (E_{ads}) of O_2 on Mn_2 dimer, the adsorption energy changes (ΔE_{ads}) compared to pure SMO slab, and the distance changes between Mn ions ($\Delta d_{Mn\text{-}Mn}$) of Mn_2 dimer after binding with Pt clusters.

	E_{ads} of O_2 (eV)	ΔE_{ads} of O_2 (eV)	$\Delta d_{Mn\text{-}Mn}$ (Å)
SMO	-0.68	/	/
Pt_1/SMO	-0.60	0.08	0.03
Pt_2/SMO	-0.25	0.43	0.09
Pt_4/SMO	-0.25	0.43	0.08
Pt_6/SMO	-0.50	0.18	0.04
Pt_8/SMO	-0.60	0.08	0.04
Pt_{20}/SMO	-0.56	0.12	0.01

Table S3. Formation energies (E_{form}) of Fe, Co and Ni dopants on SMO slab.

	Fe dopant	Co dopant	Ni dopant
E_{form} (eV)[a]	-0.60	-0.10	-1.28

[a] E_{form} is defined as:

$$E_{form} = E_{slab\text{-}X} - E_{slab} - a \times E_{XO_b} + a \times E_{MnO_2} - a \times (2-b) \times E_{O_2} / 2 \quad (27)$$

where $E_{slab\text{-}X}$ and E_{slab} are the total energies of X doped and pure slabs (X = Fe, Co. Ni), respectively. E_{MnO_2} and E_{XO_b} are total energies of the stable oxides of Mn and X elements (MnO_2, Fe_2O_3, Co_3O_4 and NiO). E_{O_2} is the energy of an O_2 molecule.

Table S4. E_{clu} of Pt_{20} clusters on pure and doped SMO slabs.

	Pure	Fe dopant	Co dopant	Ni dopant
E_{clu} (eV)	-5.20	-5.21	-5.22	-5.22